NOAA Technical Report ERL 346-AOML 21

U.S. DEPARTMENT OF COMMERCE
NATIONAL OCEANIC AND ATMOSPHERIC ADMINISTRATION
Environmental Research Laboratories

Observations of Currents and Temperatures in the Southeast Florida Coastal Zone During 1971-72

DENNIS A. MAYER
DONALD V. HANSEN

BOULDER, COLO.
JUNE 1975

U.S. DEPARTMENT OF COMMERCE
Rogers C. B. Morton, Secretary

NATIONAL OCEANIC AND ATMOSPHERIC ADMINISTRATION
Robert M. White, Administrator

ENVIRONMENTAL RESEARCH LABORATORIES
Wilmot N. Hess, Director

NOAA TECHNICAL REPORT ERL 346-AOML 21

Observations of Currents and Temperatures in the Southeast Florida Coastal Zone During 1971-72

DENNIS A. MAYER
DONALD V. HANSEN

BOULDER, COLO.
June 1975

For sale by the Superintendent of Documents, U. S. Government Printing Office, Washington, D. C. 20402

DISCLAIMER

The NOAA Environmental Research Laboratories do not approve, recommend, or endorse any proprietary product or proprietary material mentioned in this publication. No reference shall be made to the NOAA Environmental Research Laboratories, or to this publication furnished by the NOAA Environmental Research Laboratories, in any advertising or sales promotion which would indicate or imply that the NOAA Environmental Research Laboratories approve, recommend, or endorse any proprietary product or proprietary material mentioned herein, or which has as its purpose an intent to cause directly or indirectly the advertised product to be used or purchased because of this NOAA Environmental Research Laboratories publication.

CONTENTS

OBSERVATIONS OF CURRENTS AND TEMPERATURES IN THE SOUTHEAST FLORIDA COASTAL ZONE DURING 1971-72

Dennis A. Mayer
Donald V. Hansen

The long, narrow, and shallow (less than 20 m) shelf region of Southeast Florida is distinctly different from the deeper offshore water where the dominant motions are those of the Florida Current. The shallow water is primarily wind driven, but also subject to tidal motions near tidal inlets. A basic problem in determining South Florida coastal processes is that the major dynamics and, hence, the major exchange mechanisms contain so much energy at low frequency that at least 4 months of data are required for computation of reliable statistics.

In long current measurement records, the net northward motion is nearly zero. In the winter, the temperature of coastal water is less than the temperature of offshore water by about $\frac{1}{2}^{o}$C/km. This positive east-west gradient of temperature is caused by the frequently occurring cold fronts which pass over South Florida regularly in the winter.

The momentum flux that had the most spatial variation and, hence, whose divergence was also the largest, was the low frequency covariance between the north and east components of current where its sign actually changed from -26 to 20 cm^2/sec^2 over a distance of only 2 km. The resulting divergence, or Reynolds stress, was of order 10^{-4}) cm/sec^2.

1. INTRODUCTION

A description of Southeast Florida coastal processes, particularly the fluxes of material and momentum, depends on understanding the role that three major forcing mechanisms play in driving coastal waters. These have been identified as tidal inlet effects, proximity of the Florida Current, and wind effects. Together they combine to produce complex shelf water motions, especially near inlets.

Understanding exchange processes of shallow coastal waters is aided by identifying the more important fluxes and the frequency bands wherein most of their energy lies. This establishes terms in the material budget equations and the dynamical equations needed to describe the coastal processes.

The fluxes of heat and momentum computed using temperature and velocity measurements as observed in the coastal waters off southeast Florida during 1971 and 1972 are described in this report.

2. MEASUREMENT PROGRAM

Locations of current meter and wind sensor installations are shown on the chart in figure 1. Coordinates, depths, and all relevant data associated with each sensor are outlined in table 1. The measurement program consisted of two phases.

During Phase I, an attempt was made to evaluate the performance of different sensors and different types of mooring for sampling currents in the surface-wave-influenced open coastal zone and to obtain some useful data at stations 0(1) and A(1).

Phase II was designed to provide more detailed measurements of coastal processes at stations V1, V2, and V3. All stations, except for 0(1), were taut-wire moorings using the Aanderaa Model 4 Meter. Station 0(1) was a tripod supporting two ODESSA sensors (Goodheart, 1966).

Originally designed for relatively calm estuaries, ODESSA sensors have two features which detract from their utility for open coastal current measurements. Unless they are mounted on tripods to remove mooring motion, the small direction vane, in combination with low data sample rate, produces such noisy data as to be almost useless. In addition, they do not record internally but rather transmit data through an electromechanical cable (another problem source) to a surface buoy that houses a battery pack and data tapes. This, along with their weight and bulk, requires a costly investment in time and effort for the amount of useful data obtained.

ODESSA sensors were deployed at station 0(1) in February 1971 as a part of the comparison of sensors; two Aanderaa meters on a taut wire were installed at A(1) in April 1971. Each station produced less than 2 weeks of useful data. Station 0(1) had severe fouling problems after about 10 days, and the meters on A(1) were needed for another project. The fouling problems turned out to be much more severe than anticipated. In the shallow water (less than 20 m) off Southeast Florida, the current meters must be cleaned once a week unless protective coatings are applied. In Phase II, by far, the most extensive data were collected.

In Phase II, Aanderaa meters were used exclusively, and the problem of fouling was eliminated by frequent cleaning. Data were collected for 11.8 weeks (82.3 days) at V1, for 6.8 weeks (47.9 days) at V2, and 2.7 weeks (19.0 days) at V3. With the better quality data obtained in Phase II, it was possible to calculate fluxes of heat and momentum and spectra of the more important parameters. In addition, vector time series of winds and currents show qualitatively the importance of wind as a forcing mechanism for shallow water.

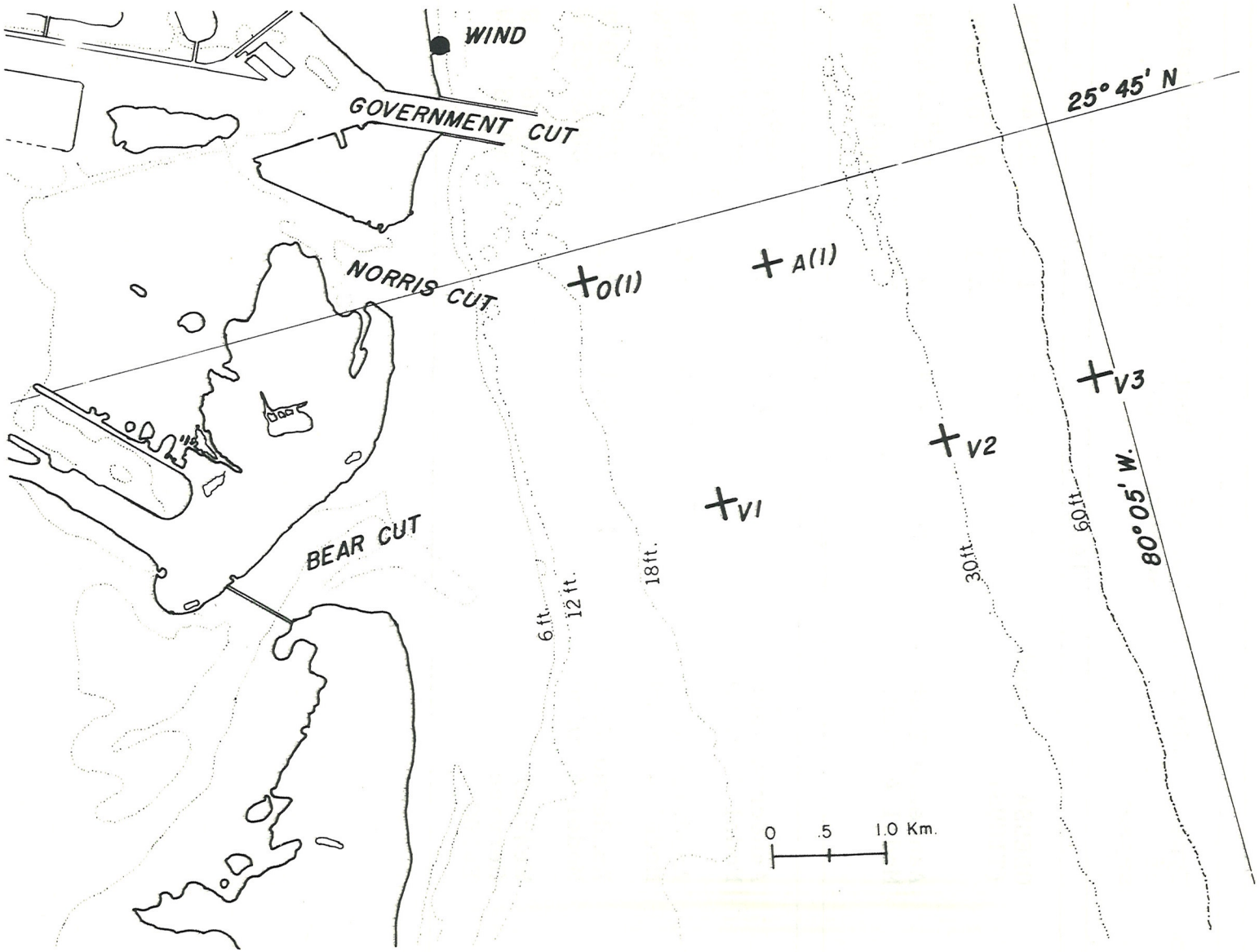

Figure 1. Location of current meter and wind sensor installation.

Table 1.

Sensor Data

Station	Type of sensor	Mooring	No. of sensors	Depth (m)	Sensor depth (m)	Coordinates
			1971			
0(1)	ODESSA (TICUS)	Tripod	2	5.5	1.7 and 4.1	25°44'54"N 80°07'30"W
A(1)	Aanderaa Model 4	Taut wire	2	8.2	2.7 and 4.9	25°44'45"N 80°06'34"W
			1972			
V1	Aanderaa Model 4	Taut wire	1	6.1	3.7	25°43'43"N 80°07'06"W
V2	Aanderaa Model 4	Taut wire	1	11.0	6.1	25°43'43"N 80°05'44"W
V3	Aanderaa Model 4	Taut wire	1	38.1	12.2	25°43'50"N 80°05'05"W
Wind	Weather Service F420C		1			25°46' N 80°08' W

3. DATA REDUCTION

Specifications of the digital filters used in analyzing the various time series are summarized in table 2a. All pertinent information for the raw time series and the various filtered series, such as start time, record length, and sample interval, is contained in table 2b.

Before computations were performed on any of the time series, all raw data were filtered and resampled at 1-hr intervals. For the 6-min sample rate at 0(1), and the 10-min sample rate at all Aanderaa stations, a 3-hr low pass was applied. The resultant series of hourly values were then used in the computations of 40-hr low- and high-passed time series.

For the more extensive data set of Phase II, statistics of the 3-hr and 40-hr low-passed data from stations V1, V2, and V3 for current components and temperature are given in table 2c together with their 70-percent confidence limits. These are fluctuation bounds within which an observation would be found 70 percent of the time for that particular data set.

4. RESULTS

4.1 Water Movements

The statistics of the time series in table 2c indicate that at all stations there is a net mean westward (shoreward) current component that diminishes eastward. The northward mean flow component has a somewhat peculiar structure, being northward at V3 and V1, as expected if coupling to the northward-flowing Florida Current is important, but surprisingly southward at V2. For the same time period as V2, V1 also shows a mean southward flow. The most probable explanation of this result is that it is due to undersampling of the low-frequency-dominated currents, even in a 6-week sampling period.

Except in the proximity of tidal inlets, the coastal waters of Southeast Florida are driven primarily by the wind and the Florida Current. In addition, the coastal processes can be partitioned into high and low frequency bands. High frequency is defined as all events having periods of less than 40 hr, and conversely for low frequency.

Histograms, in polar form, of the Phase II data were constructed for the 3- and 40-hr low-passed data and for the 40-hr high-passed data in figures 2a, 2b, and 2c. These show the frequency distribution of currents partitioned into 10^{o} increments, where the length of each is proportional

Table 2a.

Specifications of Digital Filters

Decibels	3-hr low pass		5-hr low pass	20-hr low pass	40-hr low pass	40-hr high pass
Hours (6 db)	2.5	2.9	5	16.7	37	37
Hours (20 db)	2	2	4	14	30	48
Filter length (#of points)	53	79	15	79	127	127
Sample interval Δt (min)	10	6	60	60	60	60

Table 2b.

Relevant Data for Time Series

Station	Type of filter	Start Julian Day (hr) Eastern Std. Time	Sample interval (Δt)	Number of points	Record length (hr)
		Phase I 1971			
0(1)	Raw data	57 (13.6)	6 min	2617	261.6
	3-hr LP	58 (0.0)	1 hr	248	247
	20-hr LP	60 (0.0)	6 hr	27	156
A(1)	Raw data	110 (16.67)	10 min	1955	325.7
	3-hr LP	110 (21.0)	1 hr	318	317
	20-hr LP	113 (0.0)	6 hr	38	222
Wind	5-hr LP	58 (0.0)	1 hr	248	247
	20-hr LP	60 (0.0)	6 hr	27	156
	20-hr LP	113 (0.0)	6 hr	38	222
		Phase II 1972			
V1	Raw data	48 (9.83)	10 min	11855	1975.7
	3-hr LP	49 (0.0)	1 hr	1958	1957
	40-hr LP and HP	52 (0.0)	1 hr	1823	1822
V2	Raw data	47 (13.83)	10 min	6904	1150.7
	3-hr LP	49 (0.0)	1 hr	1111	1110
	40-hr LP and HP	52 (0.0)	1 hr	976	975
V3	Raw data	95 (13.83)	10 min	2729	454.8
	3-hr LP	96 (0.0)	1 hr	441	440
	40-hr LP and HP	99 (0.0)	1 hr	306	305
Wind	5-hr LP	49 (0.0)	1 hr	1958	1957
	40-hr LP	52 (0.0)	1 hr	1823	1822

Table 2c.

Statistics of Time Series

Filter	Station	Parameter	Mean and 70% confidence limits cm/sec and °C	σ Standard deviation	Number of points
3-hr low pass	V1	v_1	2.73±.43	19.09	1958
		u_1	-2.10±.29	12.69	
		t_1	24.35±.03	1.42	
	First 1111 hr of V1	v_1	-0.41±.60	20.41	1111
		u_1	-2.25±.40	13.43	
		t_1	23.54±.03	1.01	
	V2	v_2	-1.60±.52	17.46	1111
		u_2	-1.80±.29	9.80	
		t_2	23.76±.02	0.64	
	V3	v_3	43.80±1.4	29.69	441
		u_3	-1.18±.23	4.73	
		t_3	24.61±.02	0.51	
40-hr low pass	V1	v_1	3.27±.37	15.64	1823
		u_1	-2.23±.08	3.33	
		t_1	24.34±.57	1.37	
	V2	v_2	-0.063±.46	14.22	976
		u_2	-1.87 ±.12	3.77	
		t_2	23.79 ±.01	0.60	
	V3	v_3	35.86 ±1.4	25.07	306
		u_3	-0.83 ±.09	1.60	
		t_3	24.50 ±.03	0.44	

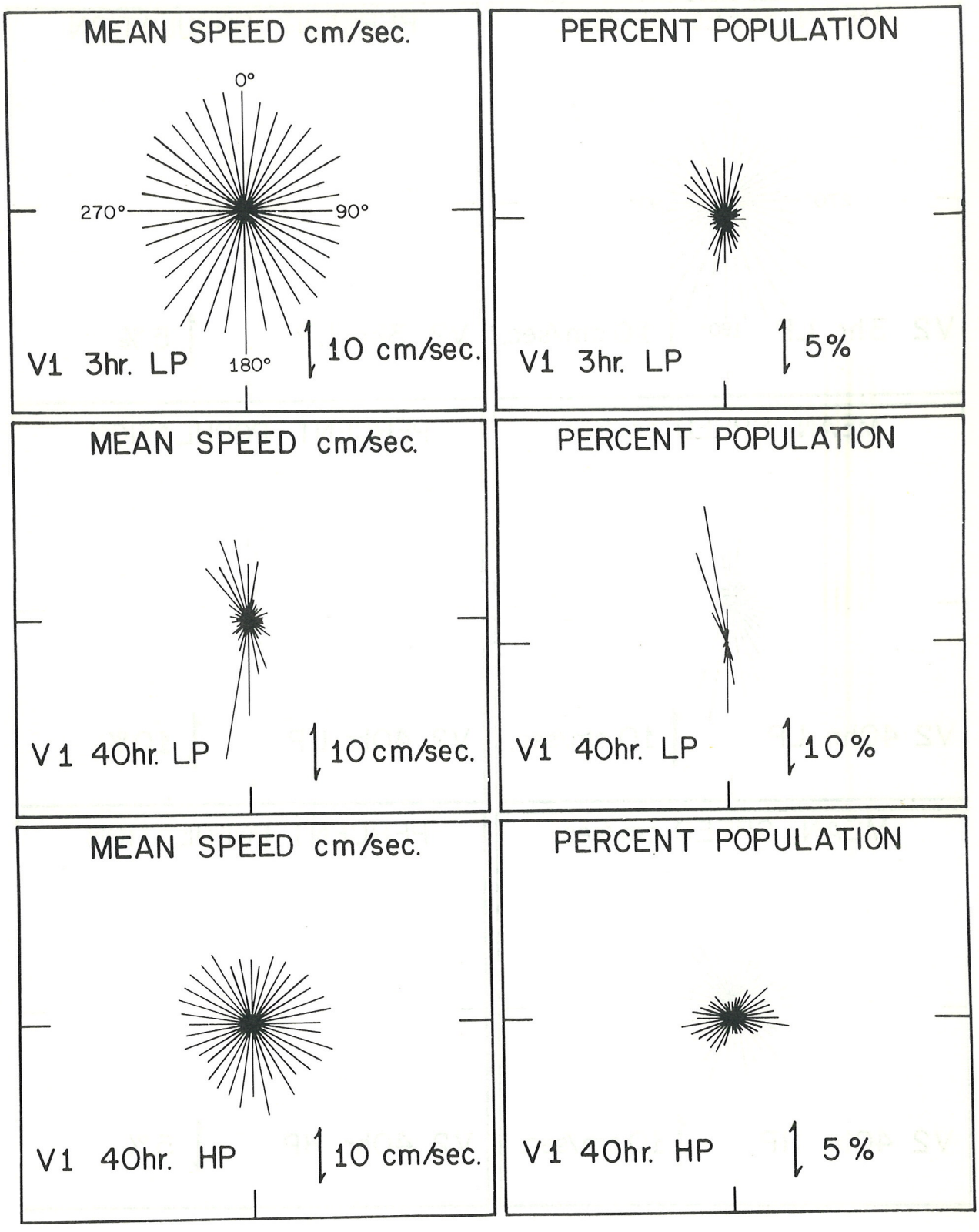

Figure 2a. 3- and 40-hr low-passed and 40-hr high-passed data at station V1.

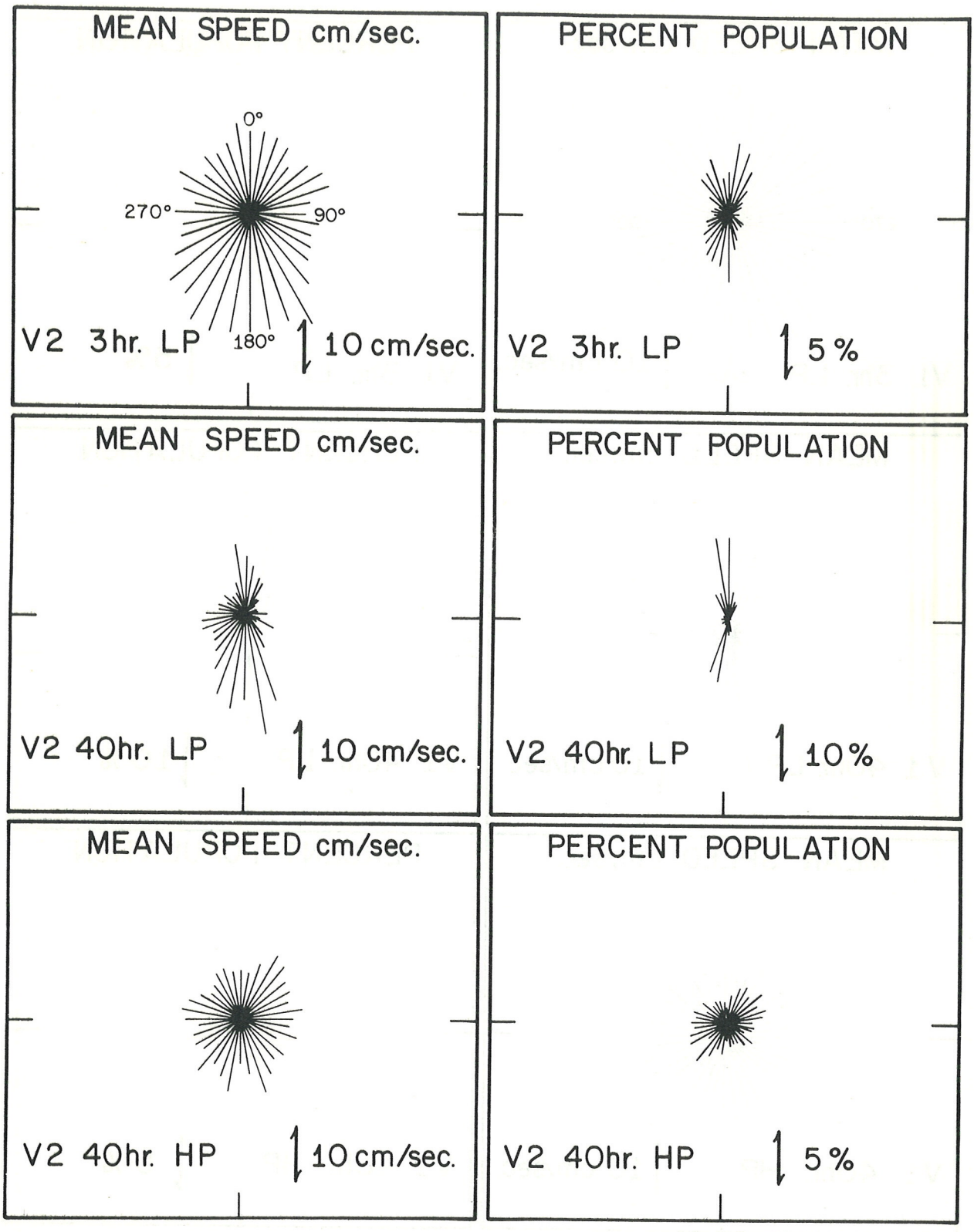

Figure 2b. 3- and 40-hr low-passed and 40-hr high-passed data at station V2.

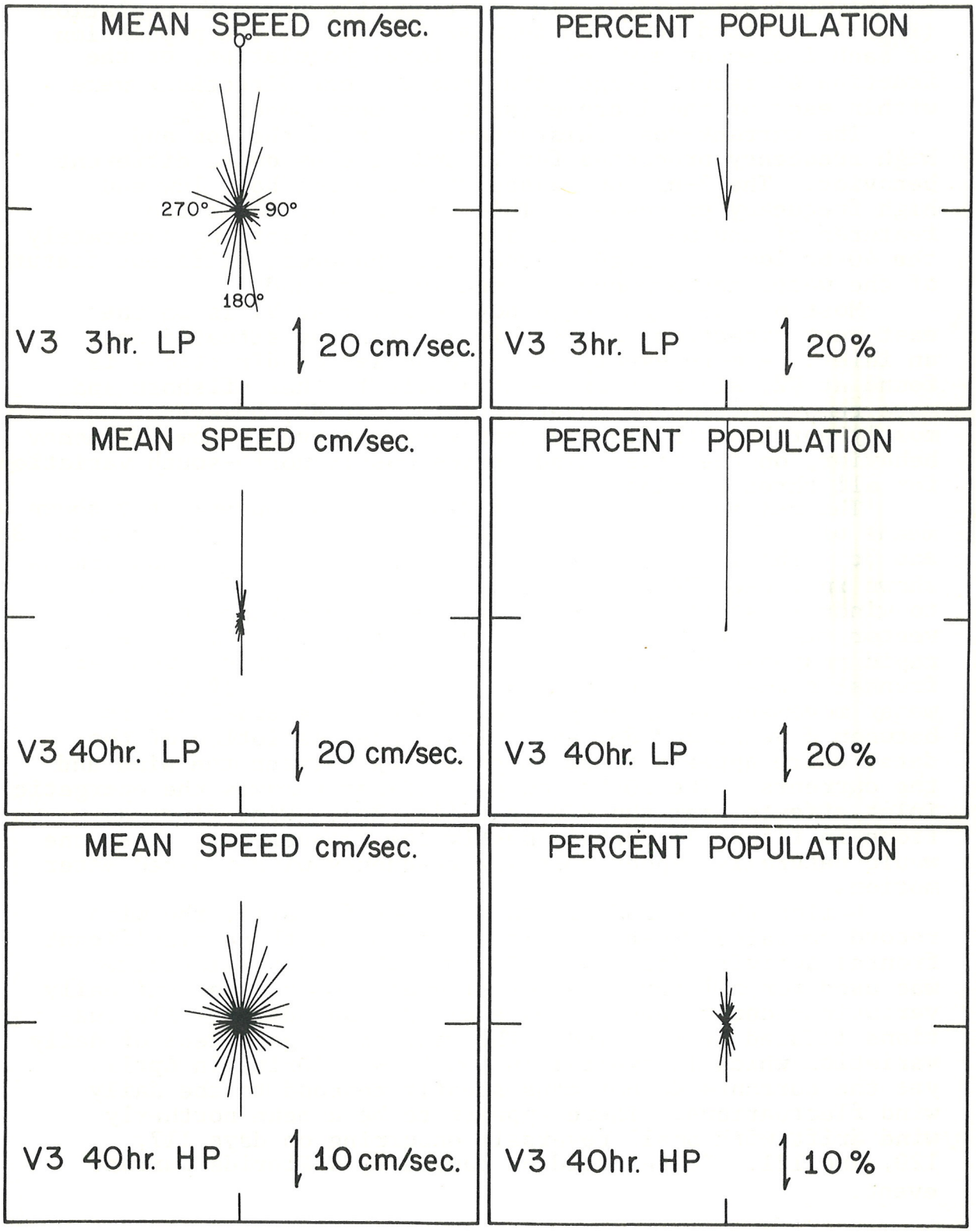

Figure 2c. 3- and 40-hr low-passed and 40-hr high-passed data at station V3.

to the mean speed (X_m). In addition, the percent population (X_{np}) is plotted for each increment. X_{np} is the population of each increment divided by the total population, or the fraction of record length that the current directions were within each of the increments at the mean speed X_m.

The current-rose (histogram) plots of the low and high frequency processes for V1 and V2 show quite different behavior. The 3-hr low-passed data combine both low and high frequency processes. This combination masks the features of the motions in each band. By plotting separately the 40-hr low- and high-passed data, however, different features of the water motions can be seen in each band.

Most of the high frequency activity at V1 is in the east-west direction, since this station was situated near an inlet. A more evenly distributed set of directions is found at V2, since it is about a mile farther offshore and more removed from the inlet effects. At V3, however, mostly north-south fluctuations were observed. Low frequency behavior, on the other hand, shows mostly north-south variations for all three stations.

The net movement past a fixed site is conveniently shown by means of a Progressive Vector Diagram (PVD), see figures 3a, 3b, and 3c. The importance of the wind as a driving mechanism is shown in these PVD's. The close relationship of currents to winds at station 0(1) is even more clearly shown by a vector time series of currents and winds (fig. 4). The rapid response of the shallow water to a classical weather frontal system resulting in an abrupt reversal of the water movement is clearly shown. Such a reversal occurs between days 63 and 65, and, within the resolution of the data, there appears to be no phase lag between the wind and the currents. The 20-hr low pass filter removes the energetic inlet effects from the PVD (see fig. 3c). Wind fluctuations in figure 3b contain mostly low frequencies; thus, one would naturally expect only low frequency wind-induced water motions.

During the period of observations for A(1), the wind record contained mostly daily variations with no significant frontal activity (fig. 5). Again a 20-hr low pass filter was used for all three vector diagrams to exclude semi-daily variations and to present more clearly any diurnal fluctuations induced by the wind. The wind has a good deal of daily variation which is typical in Southeast Florida in April, yet the currents do not consistently respond to the daily wind fluctuations. There appears to be a mean northerly wind drift with small reversals occurring on days 117, 120, and 121. These could be caused by a Florida Current event.

4.1.1 Current Shear of Stations 0(1) and A (1)

Not enough data were collected at these stations to establish a clear and consistent velocity profile. However, reasonable velocity shears and ratios (speed of upper meter divided by speed of lower meter)

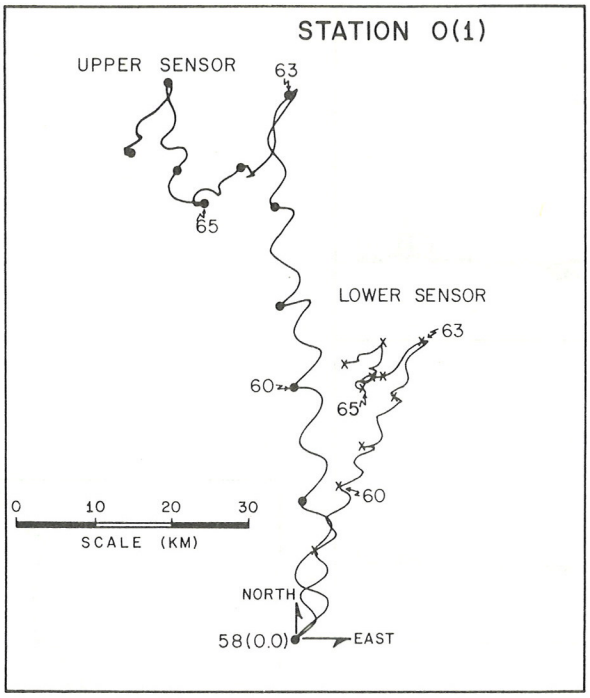

Figure 3a. 3-hr low-passed PVD of station 0(1).

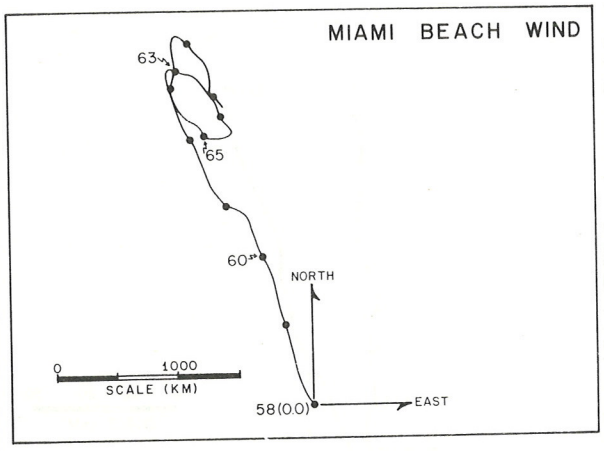

Figure 3b. 5-hr low-passed PVD of Miami Beach, Fla., wind.

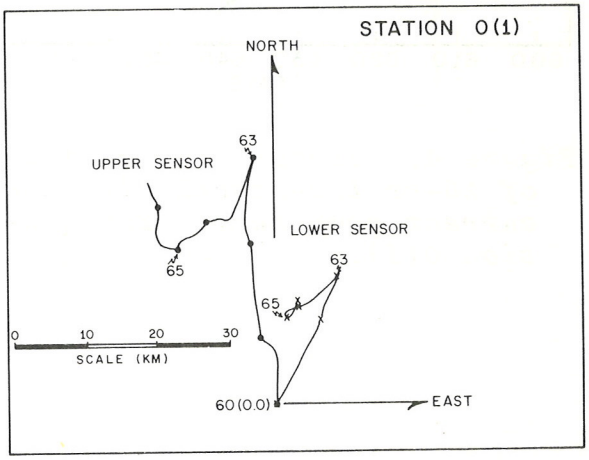

Figure 3c. 20-hr low-passed PVD of station 0(1).

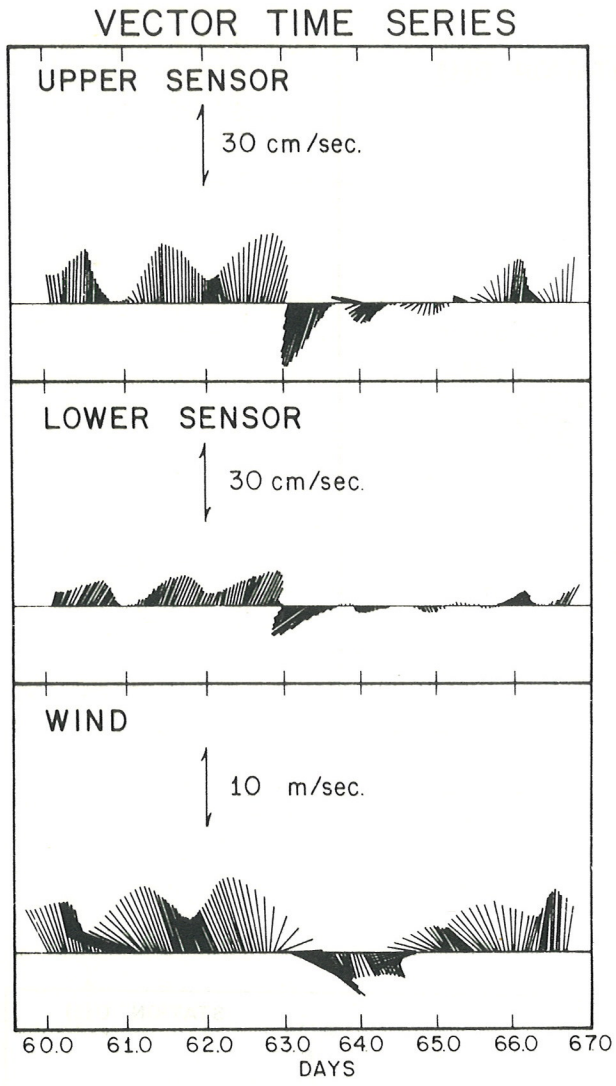

Figure 4. Vector time series of 20-hr low-passed wind and current components from station 0(1).

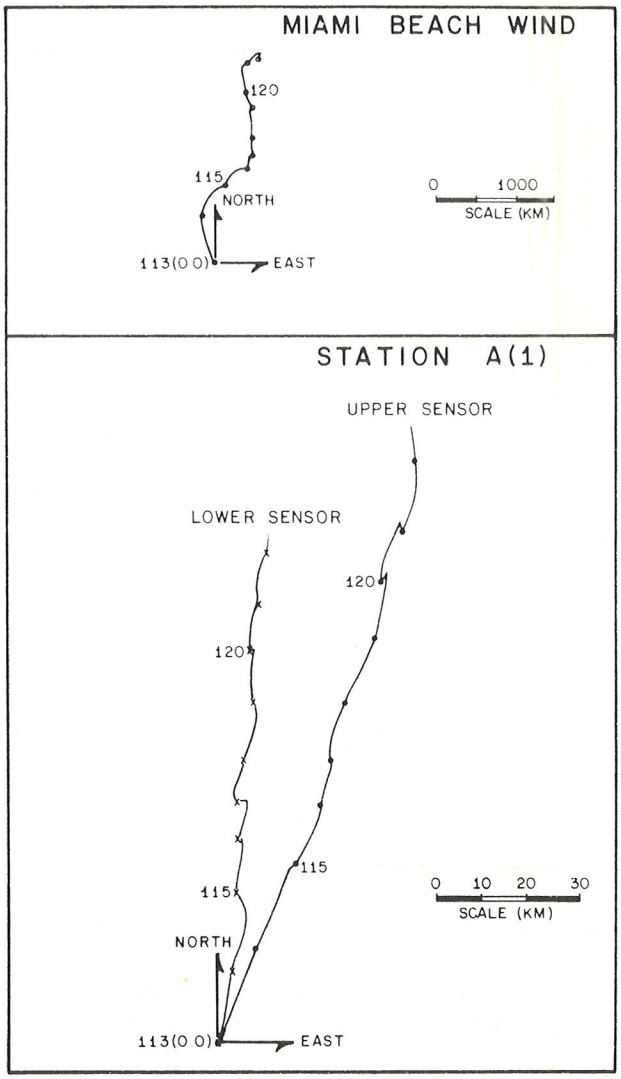

Figure 5. 20-hr low-passed PVD of station A(1).

were computed from the data. The gradients apply to those that would be found approximately at mid-depth and varied between $(10)^{-2}$ and $5(10)^{-2}$ (sec^{-1}) for 0(1). For A(1), the gradient was $(10)^{-2}$ (sec^{-1}). Velocity ratios fluctuated between 1.9 and 2.8 for 0(1). For A(1), the ratio was 1.2. These computations were based on four time intervals for 0(1) and one for A(1) where the set of the current was reasonably constant.

The degree of vertical variability was investigated by computing correlation coefficients which are the normalized covariances between the velocity components of the upper and lower sensors. These coefficients were very close to 0.90 for each of the components at A(1) and 0(1). This implies, therefore, that a single point measurement, near mid-depth, is representative of motions throughout the water column.

4.1.2 Low Frequency Motions at Stations V1, V2, and V3

Figures 6a and 6b contain PVD's assembled from the 40-hr low-passed data for V1, V2, and V3 and the Miami Beach wind. These display the motions of the low frequency or slowly varying coastal processes. The most notable aspect of the long period processes represented by the PVD's in figure 6 is that the shallow shelf water monitored by V1 and V2 appears to be quite sensitive to low frequency wind forcing. This is indicated as well in the 40-hr low-passed vector time series plots and plots of the north components of wind and currents in figures 7a and 7b.

The major low frequency features can be seen in figure 6. From days 52 to 92, the coastal water movements were parallel to the coast and oscillated with a period of about 20 days with little net movement. This corresponds quite closely to the variation of the wind. From days 92 to 115, the wind was directed much more to the north, and the current at V1 showed similar behavior.

The shorter time scale features (several days) reflect both wind and Florida Current mechanisms. In figures 6 and 7, one can see that wind events were centered about the following days: 66, 69, 80, 92, and 100. On these days, the coastal waters reversed approximately in phase with the wind direction. Mixed processes occurred over the time spans, days 52 to 54, 100 to 102, and 115 to 118. Here, except for day 100, the phase between wind and currents is not clear. In each case, the change in current direction leads the wind. It is also notable that direction changes at V1 lead those at V2, and east-west displacement is smaller at V1 than at V2. Because V3 is located near the shelf break, it is more strongly influenced by modulations of the western edge of the Florida Current which probably dominates wind-induced variability at that location. The mean direction at V3 is northward with occasional excursions southward, as is clearly shown in the histograms of currents at V3 (fig. 2) where almost 80 percent of the observations for V3 show current moving north and about 5 percent show currents moving south. Two of these

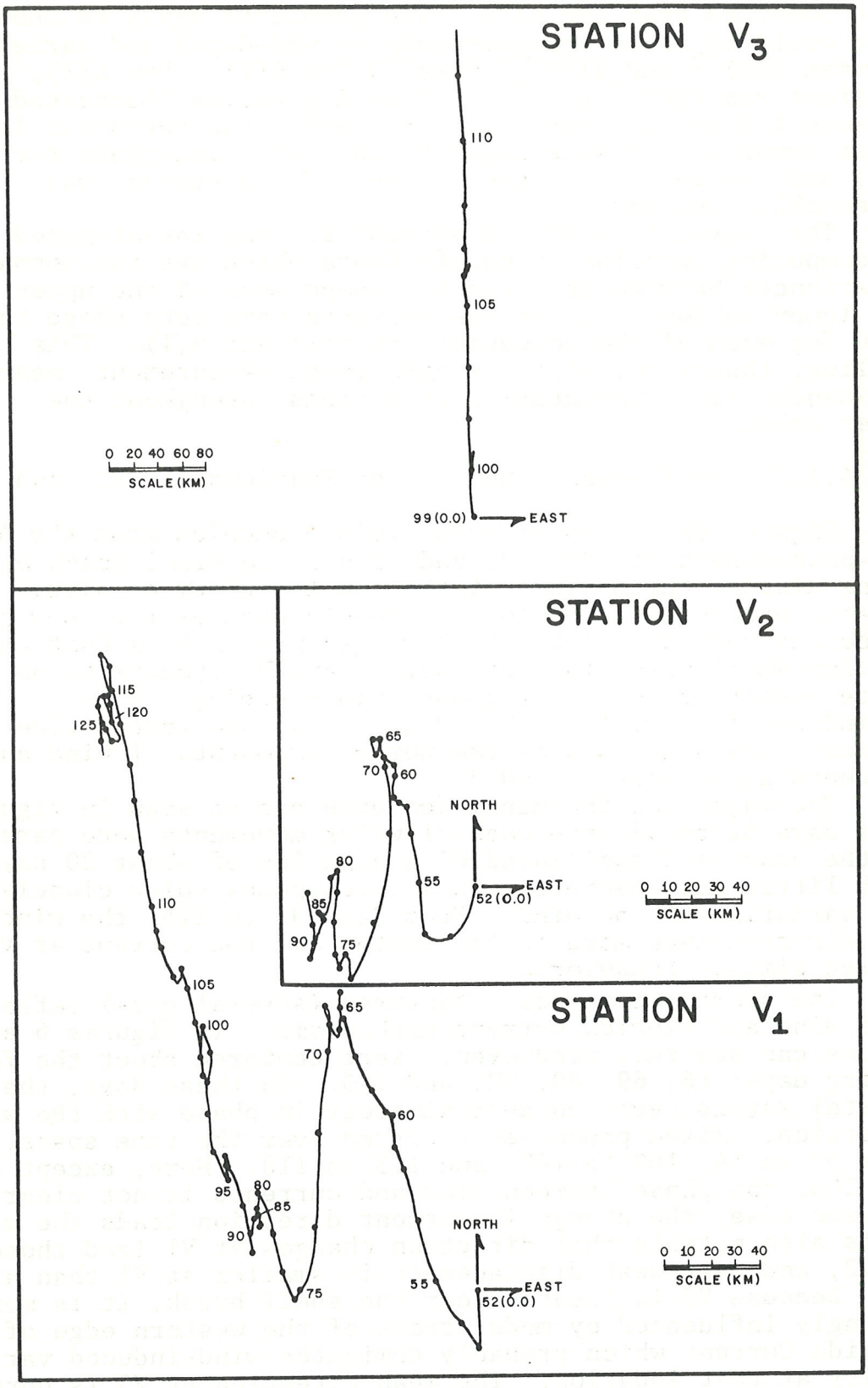

Figure 6a. 40-hr low-passed PVD's of stations V1, V2, and V3.

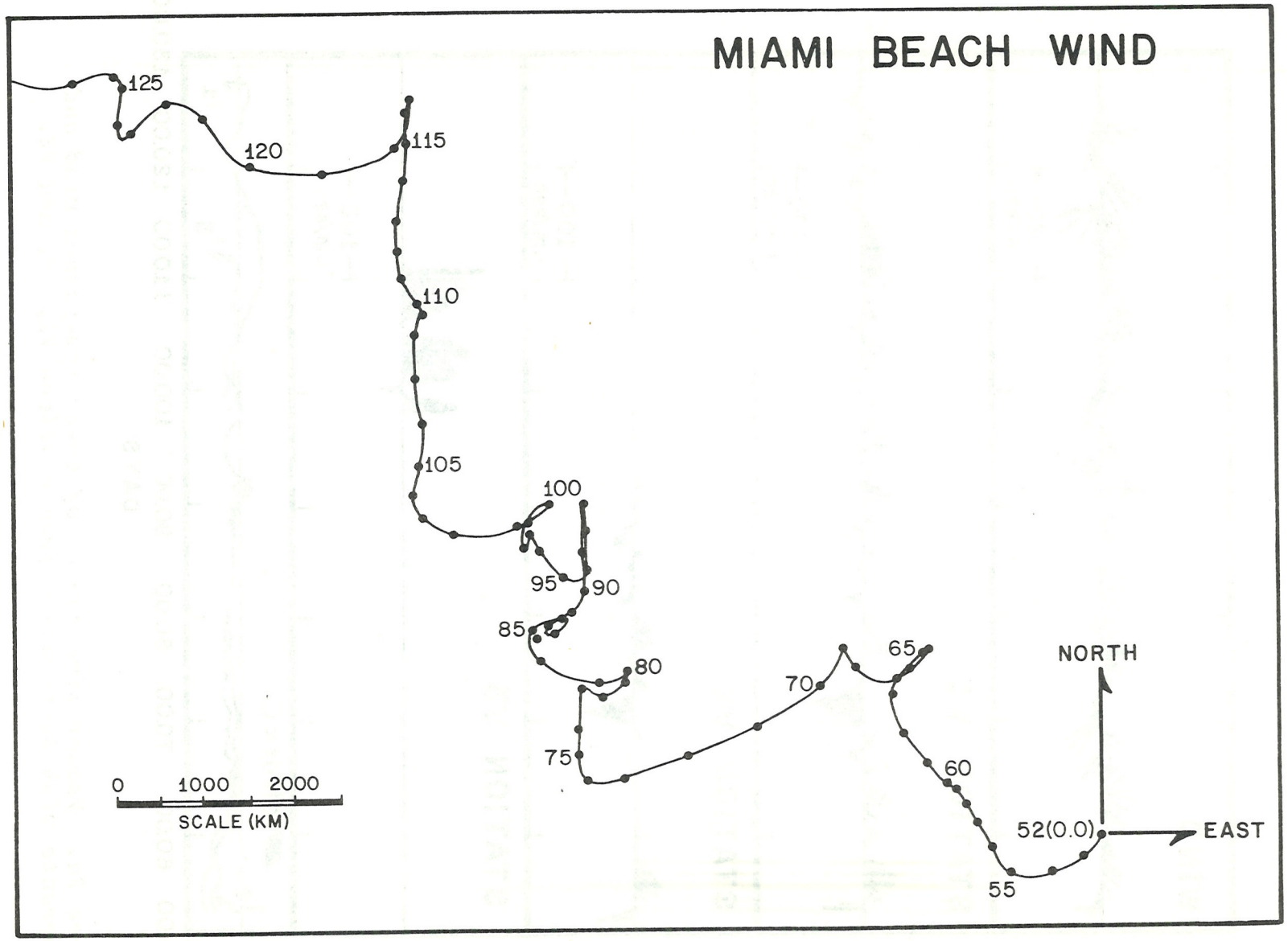

Figure 6b. 40-hr low-passed PVD of the Miami Beach, Fla., wind.

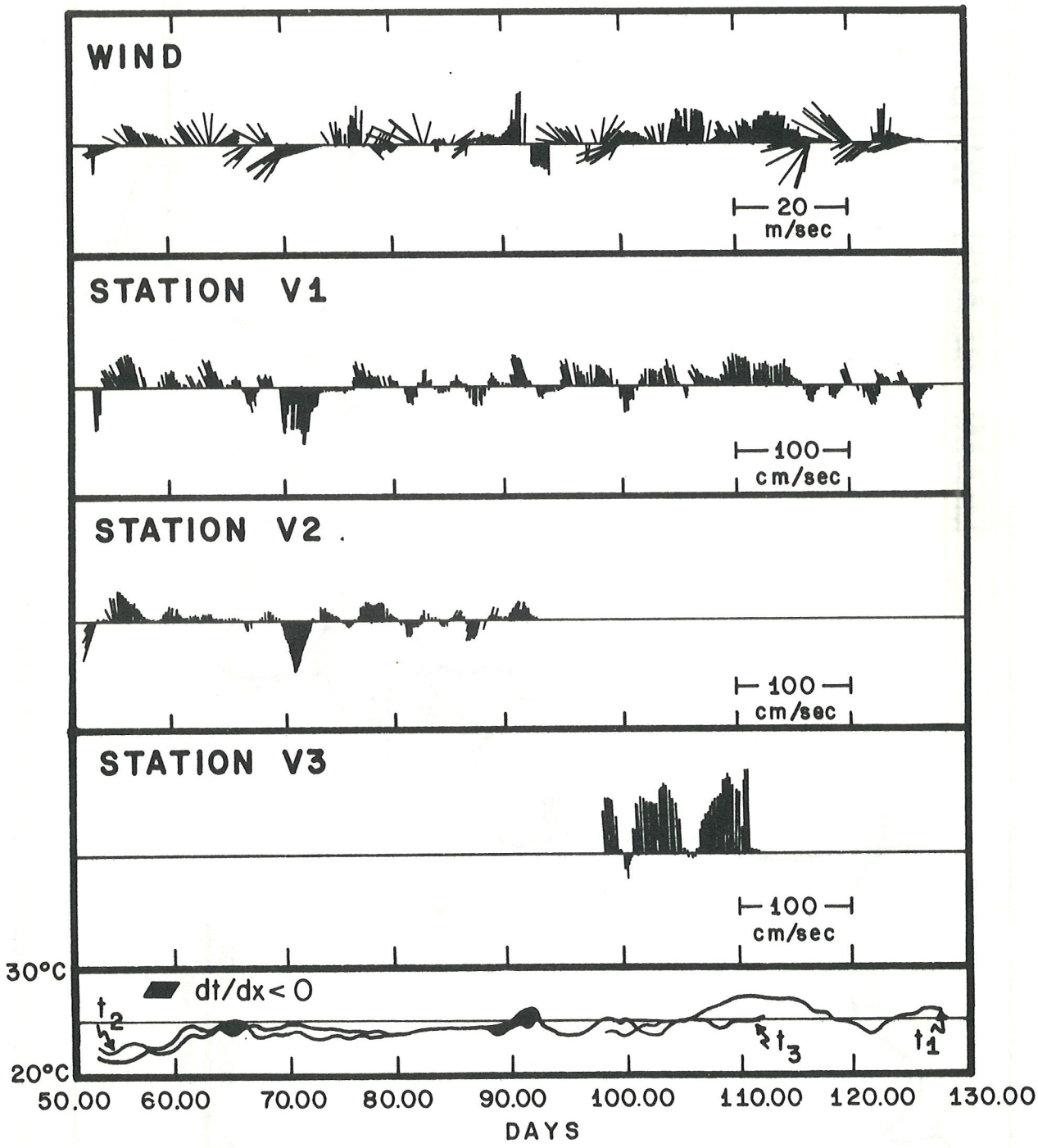

Figure 7a. Vector time series of 40-hr low-passed wind and currents with temperature from stations V1, V2, and V3.

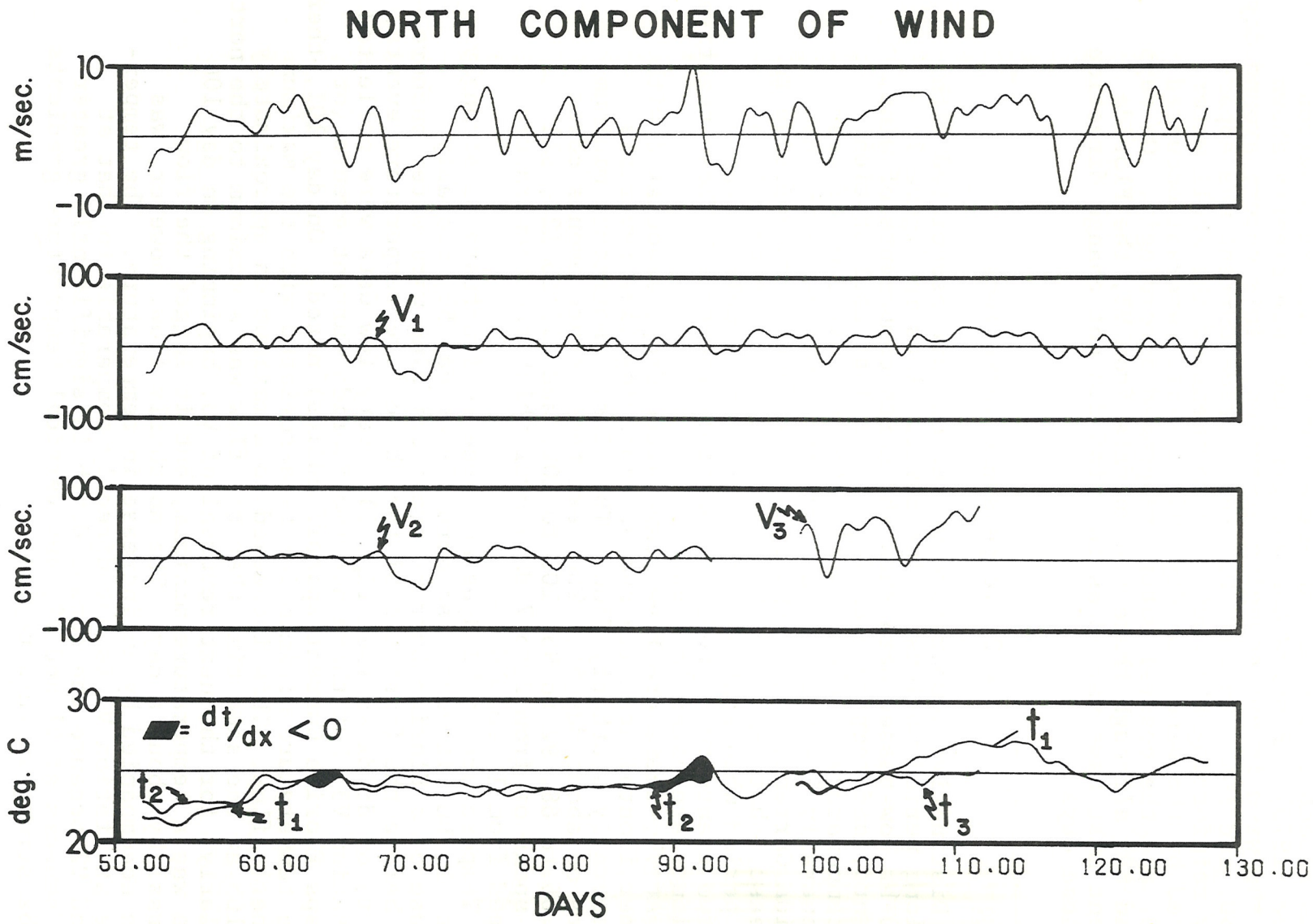

Figure 7b. 40-hr low-passed time series plots of north components of wind and currents with temperature from stations V1, V2, and V3.

southward flow events were recorded at V3 while the meter was operating (see fig. 6 and 7). These southward flow events resemble Florida Current spinoff eddies as observed by Lee (1973). Florida Current processes are clearly shown when the wind is not changing direction. This occurs around days 57, 60, and 106. On day 101, the Florida Current was apparently reinforcing the southward movement of the shelf water induced by the wind. On day 106, a small reversal occurred at V3, and the coastal waters responded accordingly. On days 57 and 60, although there are no data from V3, the Florida Current must have varied, as the wind did not change direction on these days.

4.2 Temperature Variations

Distinctive temperature variations are associated with the long period motions. Time series plots in figure 7 of 40-hr low-passed data show the north components of wind, currents, and temperatures (t_1, t_2, t_3) at each station. The temperature of the coastal water at this time of year is generally lower than near-surface temperatures in the Florida Current, hence temperature gradients are positive to the east, that is, $dt/dx > 0$. This was the case during the time period when stations V1 and V2 were sampled, except for two events that produced negative gradients. These negative gradients are noted in figure 7.

At V1, there are five temperature drops associated with weather frontal activity and accompanying flow reversals or generally southerly flow. The first temperature minimum occurs on about day 54. The next temperature events cover days 66 to 68, 92 to 95, 100 to 102, and 115 to 121, all time spans of from 2 to 7 days over which the temperature dropped from 1° to 5°C.

Temperature at V2 does not seem to fluctuate as strongly as at V1, but it does rise abruptly on day 59, probably because of a Florida Current event bringing warm water onshore. Just before the first two of the above five temperature events, $t_1 > t_2$ or $dt/dx < 0$ (see fig. 7). Very few data were collected at station V3, but there are two Florida Current events (or perhaps Florida Current spinoff eddies) noted. On day 101, there was a temperature minimum for t_3 associated with the maximum southerly flow. This increased to a maximum on approximately day 105 at the same time that the flow was a maximum to the north. Similarly, for the next reversal of V3, beginning on day 106 there was a temperature minimum, but it lagged the flow reversal by about a day. The northerly flow, however, was again accompanied by an increase in temperature. The temperature at station V3 is not directly comparable to that at V1 and V2 because the sensor depth is significantly greater than sensors at V1 and V2, and vertical temperature gradients can be strong in this region.

4.3 Spectra of Time Series

Spectra of current components and temperature and the spectra for wind are plotted in figure 8. Here can be seen the rationale for the partition between low and high frequency processes at 40 hr or 0.6 c/day. The strong semidiurnal signal (inlet effects) for the east components of current is clearly seen as well as the fairly distinct diurnal signal for the temperature (diurnal heating) and wind (sea breeze). The broad band of energy in the low frequency range for the north components or current and wind is also evident.

4.4 Fluxes of Heat and Momentum

The data from Phase II have been used to evaluate the fluxes of heat and momentum. Here heat is used as an example. It is convenient to represent the time series in terms of three important time scales as

$$W = \langle W \rangle + \overline{W} + W',$$

where W = (u,v) for velocity, and

$$t = \langle t \rangle + \overline{t} + t'$$

for temperature.

The symbol $\langle\rangle$ is a time average over the record length; thus $\langle w \rangle$ is the mean for the record length W_m. The overbarred terms, $\overline{W}$ and $\overline{t}$, are 40-hr low-passed data minus the mean and represent the slowly varying or low frequency processes. Terms like W' and t' are 40-hr high-passed data and represent the rapidly varying or high frequency processes. Heat flux over the record length is expressed as

$$\langle Wt \rangle = \langle W \rangle \langle t \rangle + \langle \overline{W}\,\overline{t} \rangle + \langle W't' \rangle , \qquad (1a)$$

and the momentum flux over the record length is expressed as

$$\langle W\ W \rangle = \langle W \rangle \langle W \rangle + \langle \overline{W}\ \overline{W} \rangle + W'W'. \qquad (1b)$$

The terms $\langle WW \rangle$ are usually called Reynolds stresses. The units of the heat flux terms in equation (1a) are heat flow per unit area. Its divergence is proportional to the sum of heat storage rate per unit volume and vertical flux. Similarly, the terms in equation (1b) are proportional to the transport of momentum. Statistics of the time series and flux series are tabulated in tables 2 and 3 with the fluctuation bounds around the means that correspond to approximately 70-percent confidence limits.

The cross-terms involving $\langle W'\overline{t} \rangle$ and $\langle \overline{W}\ t' \rangle$ are conventionally regarded as contributing only an insignificant amount to

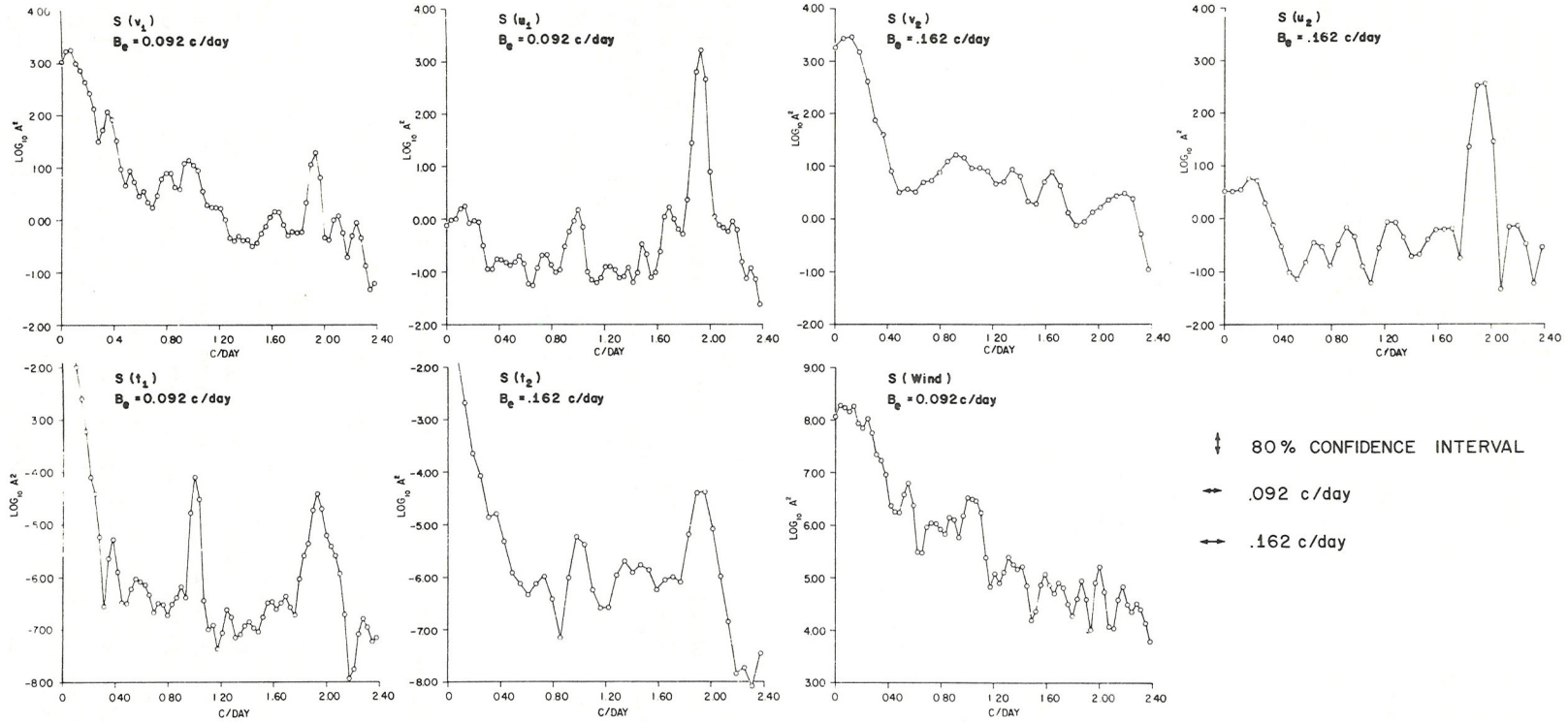

Figure 8. Spectra of north and east components of currents from stations V1 and V2, spectra of temperature from V1 and V2, and spectra of north component of wind.

Table 3.

Statistics of Heat and Momentum Flux Time Series

Parameter	Length of series	Mean and 70% confidence limits	Standard deviation
$\bar{v}_1\bar{t}_1$	976	-1.04 ± 0.57	17.92
$\bar{u}_1\bar{t}_1$	976	0.89 ± 0.17	5.26
$\bar{v}_2\bar{t}_2$	976	-2.46 ± 0.33	10.37
$\bar{u}_2\bar{t}_2$	976	0.91 ± 0.12	3.80
$\bar{v}_1\bar{t}_1$	1823	2.95 ± 0.54	23.06
$\bar{u}_1\bar{t}_1$	1823	0.75 ± 0.14	5.75
$v_1't_1'$	976	-0.25 ± 0.12	3.68
$u_1't_1'$	976	-1.01 ± 0.14	4.45
$v_2't_2'$	976	-.21 ± 0.07	2.26
$u_2't_2'$	976	0.12 ± 0.07	2.04
$v_1't_1'$	1823	-0.18 ± 0.07	3.11
$u_1't_1'$	1823	-0.61 ± 0.09	3.72
$\bar{v}_1\bar{v}_1$	976	299.43 ± 15.60	487.33
$\bar{v}_1\bar{u}_1$	976	-26.15 ± 2.00	62.51
$\bar{u}_1\bar{u}_1$	976	11.69 ± 0.62	19.27
$\bar{v}_2\bar{v}_2$	976	202.26 ± 11.97	373.83
$\bar{v}_2\bar{u}_2$	976	19.61 ± 2.53	79.11
$\bar{u}_2\bar{u}_2$	976	14.18 ± 0.98	30.75
$\bar{v}_1\bar{v}_1$	1823	244.56 ± 9.50	405.55
$\bar{v}_1\bar{u}_1$	1823	-26.16 ± 1.29	55.18
$\bar{u}_1\bar{u}_1$	1823	11.11 ± 0.44	18.84
$v_1'v_1'$	976	106.49 ± 6.25	195.12
$v_1'u_1'$	976	14.74 ± 5.27	164.62
$u_1'u_1'$	976	172.85 ± 8.19	255.72
$v_2'v_2'$	976	84.14 ± 6.10	190.42
$v_2'u_2'$	976	15.52 ± 3.87	120.89
$u_2'u_2'$	976	80.01 ± 4.37	136.66
$v_1'v_1'$	1823	97.34 ± 4.28	182.82
$v_1'u_1'$	1823	9.42 ± 3.45	147.34
$u_1'u_1'$	1823	149.07 ± 5.36	229.00

flux balances because of low correlation, and on this basis were neglected. Their evaluation is also possible for these data, and indeed they are found to be small; however, their large variances produce confidence limits troublesomely large compared to the mean fluxes of the high frequency terms $\langle W't' \rangle$.

For components of the flux divergences, it was possible to compute only east-west derivatives, since the current meters were oriented in an east-west direction.

The east-west divergence component is

$$\frac{\partial P}{\partial X} + \frac{P}{h}\frac{\partial h}{\partial X} = \frac{1}{h} \nabla_x . (Ph) ,$$

where P is the flux density and h is the depth. For these calculations, the above derivatives can be approximated by

$$\frac{P_2 - P_1}{\Delta X} + \frac{P_2 + P_1}{2} \quad (3 \times 10^{-6}) .$$

The following divergences of heat and momentum have been computed

$$\nabla . \left[\langle (u-u_m)(t-t_m) \rangle h \quad , \langle (v-v_m)(u-u_m) \rangle h, \right.$$
$$\left. \langle (u-u_m) \ (u-u_m) \rangle h \right],$$

where

$$\langle (u-u_m)(t-t_m) \rangle = \langle \bar{u} \ \bar{t} \rangle + \langle u't' \rangle$$

$$\langle (v-v_m) \ (u-u_m) \rangle = \langle \bar{v} \ \bar{u} \rangle + \langle v'u' \rangle$$

$$\langle (u-u_m)(u-u_m) \rangle = \langle \bar{u} \ \bar{u} \rangle + \langle u'u' \rangle .$$

A schematic of the more important flux terms that result in the most significant divergences is given in figure 9.

4.4.1 Heat Fluxes

During the months of November through April, measurable temperature gradients exist between the Florida Current and the coastal waters, making temperature an indicator for inshore water and heat flux a potential measure of coastal exchange rates. Heat flux spectra are shown in figure 10.

In general, slowly varying processes transport heat offshore, and the high frequency processes transport heat shoreward. Integrated values for the long period processes are

$$\langle \bar{u}_1 \bar{t}_1 \rangle = 0.89 \pm 0.17 \ (^{o}C \text{ cm/sec})$$

and

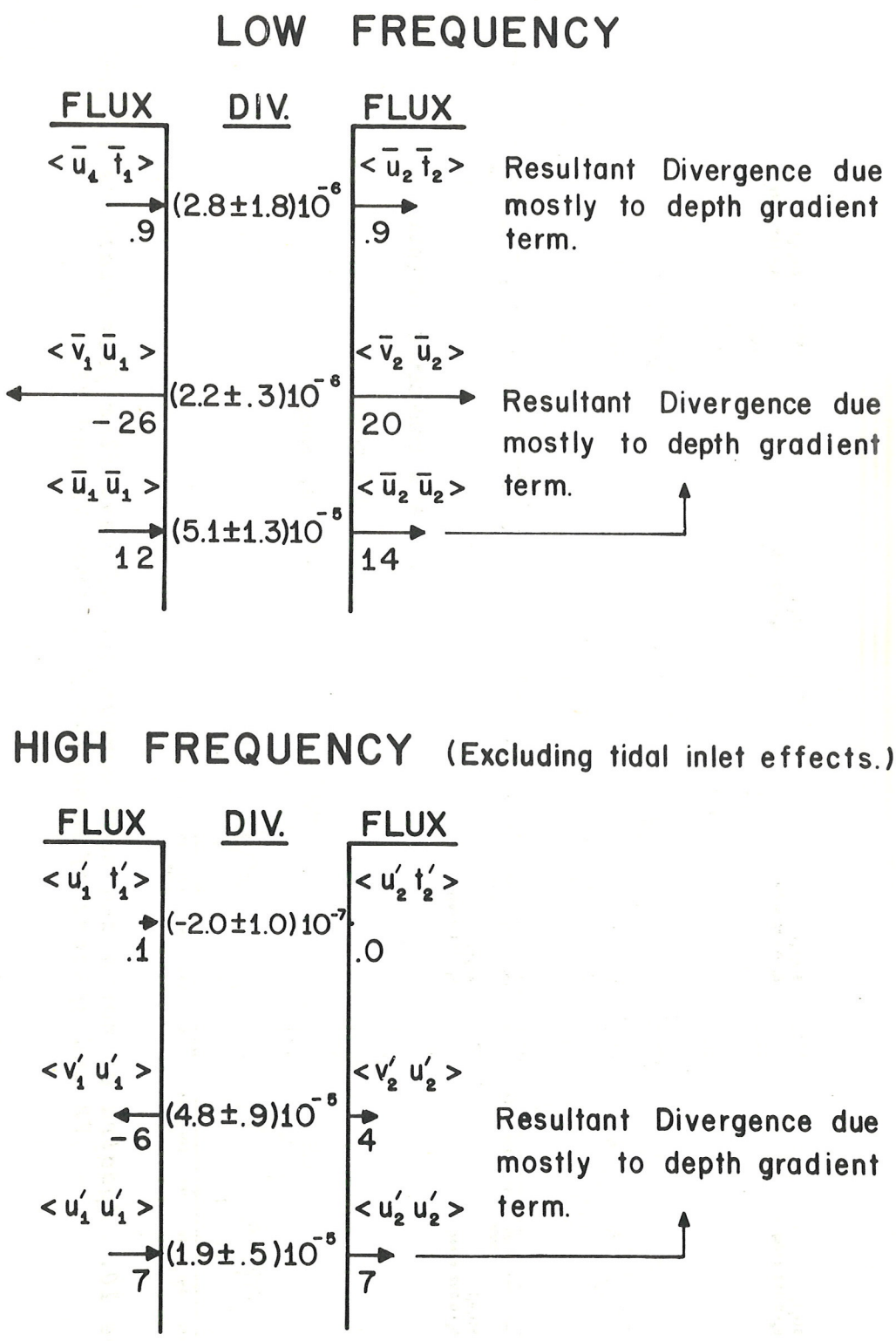

Figure 9. Schematic of the more important flux and divergence terms.

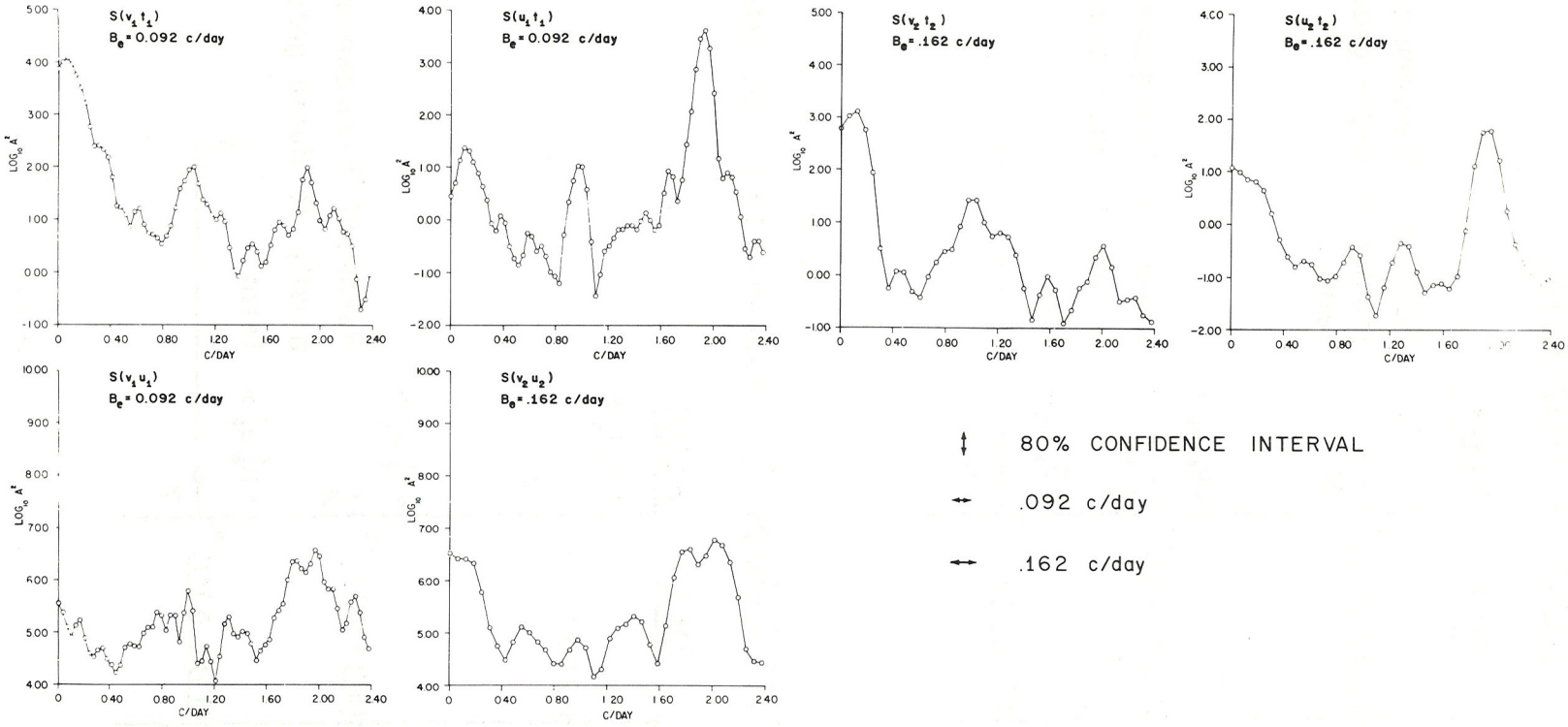

Figure 10. Spectra of north and east components of heat flux from stations V1 and V2 and spectra of momentum flux from V1 and V2.

$$\langle \bar{u}_2 \bar{t}_2 \rangle = 0.91 \pm 0.12 \ (^{o}C \text{ cm/sec}),$$

yielding a divergence of

$$\frac{\partial}{\partial x} \left(\langle \bar{u}\ \bar{t} \rangle \right) \approx (0.01 \pm 0.15)\ (10)^{-5}\ (^{o}C/\text{sec})$$

and

$$\langle \bar{u}\ \bar{t} \rangle \frac{1}{h} \frac{\partial h}{\partial x} \approx (0.27 \pm 0.04)\ (10)^{-5}\ (^{o}C/\text{sec}),$$

with the total being

$$\frac{1}{h} \nabla_x . (\langle \bar{u}\ \bar{t} \rangle h) \approx (0.28 \pm 0.18)\ (10)^{-5}\ (^{o}C/\text{sec}). \quad (2)$$

High frequency heat transports show that

$$\langle u_1' t_1' \rangle = -1.01 \pm 0.14 \ (^{o}C \text{ cm/sec})$$

and

$$\langle u_2' t_2' \rangle = 0.12 \pm 0.07 \ (^{o}C \text{ cm/sec}),$$

yielding a divergence of

$$\frac{\partial}{\partial x} \left(\langle u't' \rangle \right) \approx (0.56 \pm 0.11)\ (10)^{-5}\ (^{o}C/\text{sec})$$

and

$$\langle u't' \rangle \frac{1}{h} \frac{\partial h}{\partial x} \approx (-0.14 \pm 0.03)\ (10)^{-5}\ (^{o}C/\text{sec}),$$

with the total being

$$\frac{1}{h} \nabla_x . (\langle u't' \rangle h) \approx (0.42 \pm 0.14)\ (10)^{-5}\ (^{o}C/\text{sec}) \quad (3)$$

This divergence (3) was calculated without removing the tidal currents. This is especially significant near tidal inlets, and, of course, stations V1 and V2 are directly east of the Bear Cut inlet. An estimate of the importance of flux terms for areas where there are no inlets, the more typical coastal area, can be obtained by applying a 20-hr low pass filter to the 40-hr high-passed series and then forming the fluxes and calculating the statistics of these product series. This has been done for the momentum fluxes as well, and the results are tabulated in table 4. This bandpassing admits processes whose periods lie between 20 and 30 hr, thereby excluding the major semidiurnal tidal effects.

Recalculating equation (3) from the statistics in table 4, the high frequency transports are

Table 4.

Fluxes with Semi-Daily Fluctuations
Removed Before Forming Product Series

Parameter	Length of series	Mean and 70% confidence limits	σ
$v_1 t_1$	889	0.02 ± 0.03	1.01
$u_1 t_1$	889	0.08 ± 0.01	0.35
$v_2 t_2$	889	-0.06 ± 0.02	0.61
$u_2 t_2$	889	0.01 ± 0.01	0.29
$v_1 t_1$	1736	-0.06 ± 0.02	0.99
$u_1 t_1$	1736	0.05 ± 0.01	0.46
$v_1 v_1$	889	37.75 ± 2.32	69.31
$v_1 u_1$	889	-5.88 ± 0.66	19.59
$u_1 u_1$	889	7.30 ± 0.33	9.95
$v_2 v_2$	889	24.39 ± 1.91	56.91
$v_2 u_2$	889	4.25 ± 0.73	21.66
$u_2 u_2$	889	6.86 ± 0.42	12.64
$v_1 v_1$	1736	36.95 ± 1.64	68.34
$v_1 u_1$	1736	-7.82 ± 0.65	27.13
$u_1 u_1$	1736	8.84 ± 0.38	15.79

$$\langle u_1' t_1' \rangle = 0.08 \pm 0.01 \ (^{o}C \text{ cm/sec})$$

and

$$\langle u_2' t_2' \rangle = 0.01 \pm 0.01 \ (^{o}C \text{ cm/sec}),$$

yielding a divergence of

$$\frac{\partial}{\partial x} (\langle u't' \rangle) \approx (-0.03 \pm 0.01) \ (10)^{-5} (^{o}C/\text{sec})$$

and

$$\langle u't' \rangle \frac{1}{h} \frac{\partial h}{\partial x} \approx (0.01 \pm 0.00) \ (10)^{-5} (^{o}C/\text{sec}),$$

with the total being

$$\frac{1}{h} \nabla_x . (\langle u't' \rangle h) = (-0.02 \pm 0.01) \ (10)^{-5} (^{o}C/\text{sec}),$$

which is more than an order of magnitude smaller than equation (3).

The longshore heat transport consists of a fairly stationary southward high frequency component and a nonstationary long period component. The latter result is consistent with the rather wide band forcing of the coastal waters by the wind and the Florida Current.

4.4.2 Momentum Fluxes

For the momentum fluxes tabulated in tables 3 and 4, two major features can be identified, one with the slowly varying processes and the other with the high frequency terms. Spectra of momentum fluxes are shown in figure 10. The contribution of slowly varying processes to the cross terms $\langle \bar{V} \bar{U} \rangle$ has great spatial variation. Table 5 and figure 9 summarize the most important flux and divergence terms.

4.5 Limitations of Divergence Calculations

Since the means summarized in table 2 are unstable, though they were computed from record lengths of 1½ to 3 months, the flux calculations of heat and momentum and hence their divergences are suspect. Stable statistics of Southeast Florida coastal processes require record lengths of at least 4 months. The summary of divergence calculations in table 5, however, does hint at the most important terms for the diffusion of heat and momentum.

Table 5

Summary of Flux Divergences

Low frequency		
$\frac{1}{h} \nabla_x \cdot (\langle \bar{u}\ \bar{t} \rangle h)$	$(2.8 \pm 1.8)\ (10)^{-6}$	$(^{o}C/sec)$
$\frac{1}{h} \nabla_x \cdot (\langle \bar{v}\ \bar{u} \rangle h)$	$(2.2 \pm 0.3)\ (10)^{-4}$	(cm/sec^2)
$\frac{1}{h} \nabla_x \cdot (\langle \bar{u}\ \bar{u} \rangle h)$	$(5.1 \pm 1.3)\ (10)^{-5}$	(cm/sec^2)

High frequency					
	Including tidal inlet effects			Excluding tidal inlet effects	
$\frac{1}{h} \nabla_x \cdot (\langle u't' \rangle h)$	$=(4.2 \pm 1.4)\ (10)^{-6}$	$(^{o}C/sec)$	$(-2.0 \pm 1.0)\ (10)^{-7}$		$(^{o}C/sec)$
$\frac{1}{h} \nabla_x \cdot (\langle v'u' \rangle h)$	$=(4.9 \pm 5.9)\ (10)^{-5}$	(cm/sec^2)	$(4.8 \pm 0.9)\ (10)^{-5}$		(cm/sec^2)
$\frac{1}{h} \nabla_x \cdot (\langle u'u' \rangle h)$	$=(8.4 \pm 0.8)\ (10)^{-4}$	(cm/sec^2)	$(1.9 \pm 0.5)\ (10)^{-5}$		(cm/sec^2)

5. SPECTRAL ESTIMATES

Spectra with 15^{o} of freedom and a Tukey lag window were calculated for all the parameters, including heat and momentum fluxes (Jenkins and Watts, 1969). If n represents the number of degrees of freedom, T the record length, and M the number of lags, then n = 2BT, where the effective bandwidth B_e for a Tukey lag window is 1.33 (1/M) or 2.67 (1/2M), almost three times the resolution frequency 1/2M, and almost three times the effective bandwidth of a rectangular window. The variance for each spectral estimate is reduced by 86.5 percent compared with the variance of the sample spectrum. In other words, the variance of the spectral estimates is only 13.5 percent of the variance of the sample spectrum which is just a simple Fourier transform. A sample spectral component X_n is defined as

$$X_n = \left| \frac{1}{T} \int_{-T/2}^{T/2} x(t) e^{-2\pi f t} \, dt \right| ,$$

where X_n is the amplitude of the nth frequency component of the time series x(t). The variance ratio for a Tukey lag window is 0.75 (M/T)., and with 15^{o} of freedom, M/T = 0.18 and the variance ratio (0.75) x (0.18) = 0.135.

With 15^{o} of freedom, fluctuation bounds or a confidence interval, within which each of the spectral estimates will lie with a certain probability, may be defined. For each of the spectral plots, this confidence interval was chosen as 80 percent and its limits are shown on each of the plots in figures 8 and 10 with the effective bandwidth B_e. The ordinates of all the spectral plots are $\log_{10}$ (amplitude squared), making the confidence interval for each of the estimates constant.

5.1 Stability and Stationarity

The stability of the spectra may be evaluated by comparing estimates with different degrees of freedom, and the question of stationarity may be addressed by looking at a time history of the spectral estimates.

The question of stationarity was approached by taking the north component of current at station V1, together with the east-west heat flux at V1, and the north component of wind, and breaking the series up into five chunks or segments of 1024 points or hours for each. Each chunk was a data block shifted 240 hours from the previous block, except for the last chunk which represented less than a 240-hr shift. Thus, for each parameter, five spectra were computed, each of which was about 77-percent redundant, or contained an overlap of 77 percent of the points of the previous chunk. The amount of redundancy involved here produced gradual changes in the spectral estimates. These are shown in figures 11a, 11b, and 11c where five spectra were computed for the north component of current, east-west heat flux at V1, and the north component of

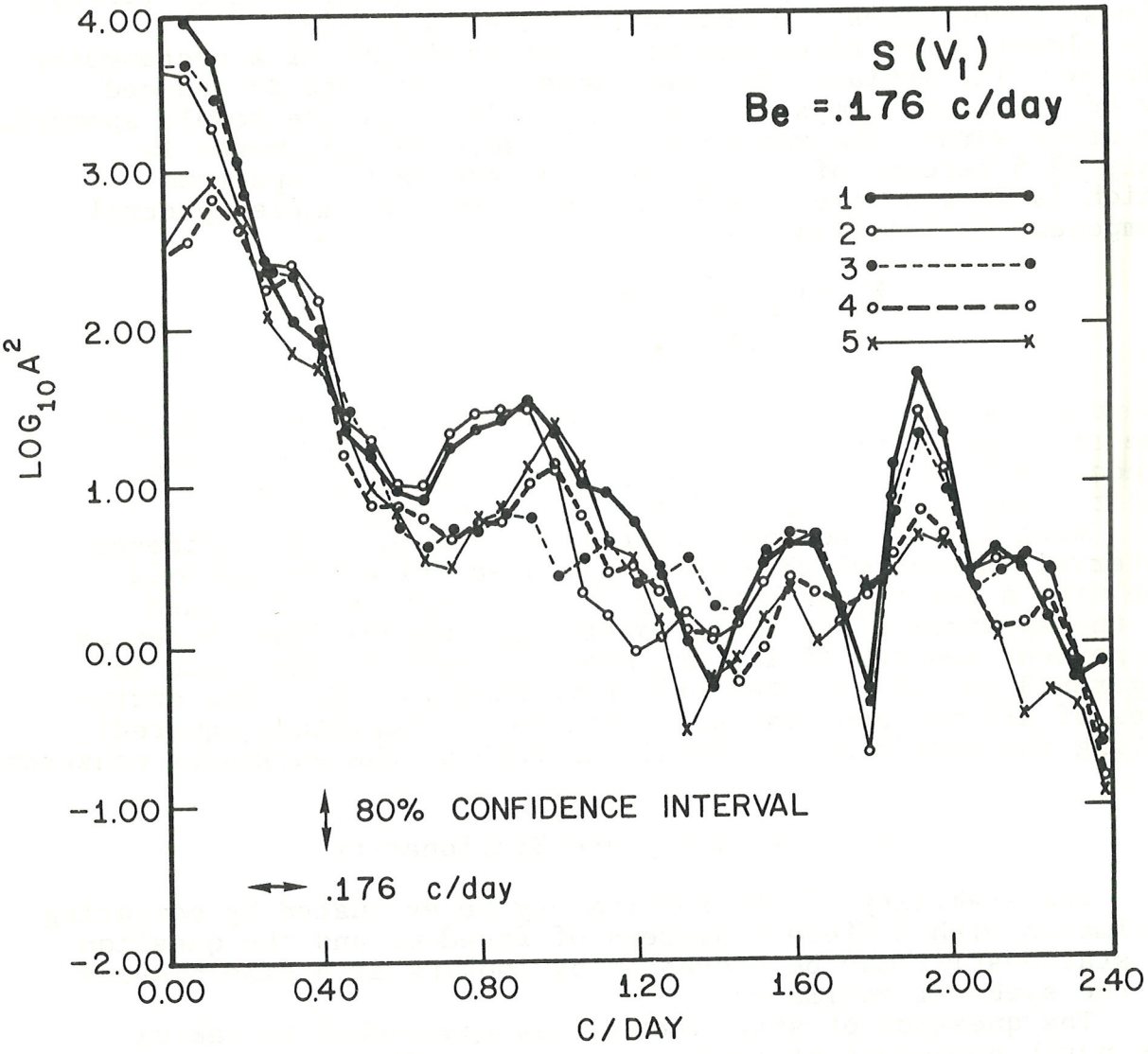

Figure 11a. Spectra of north component of current at station V1 for record lengths of 1024 hours. Each record length overlaps its adjacent record length by 77%.

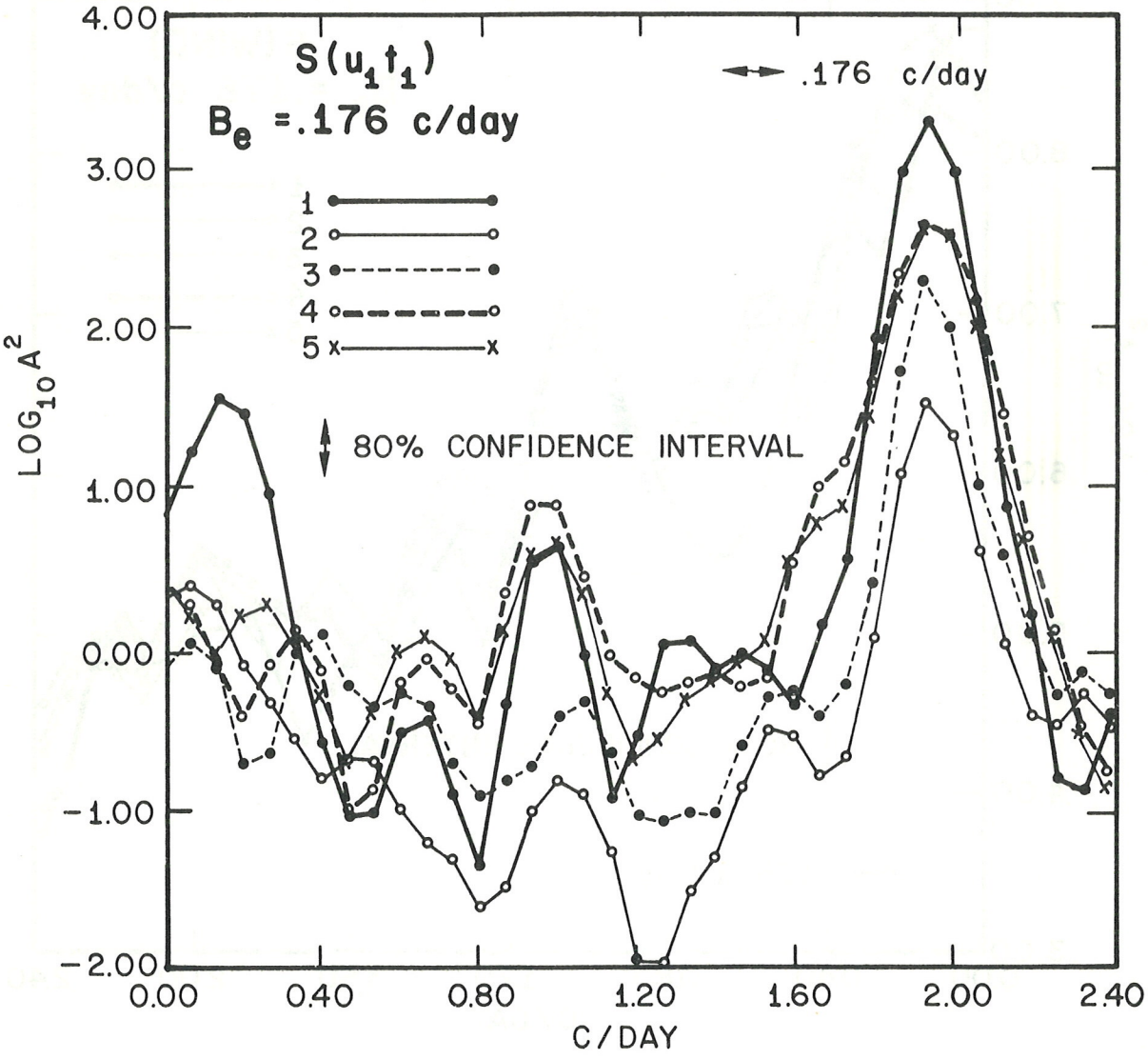

Figure 11b. Spectra of east-west heat flux at station V1 for five record lengths of 1024 hours. Each record length overlaps its adjacent record length by 77%.

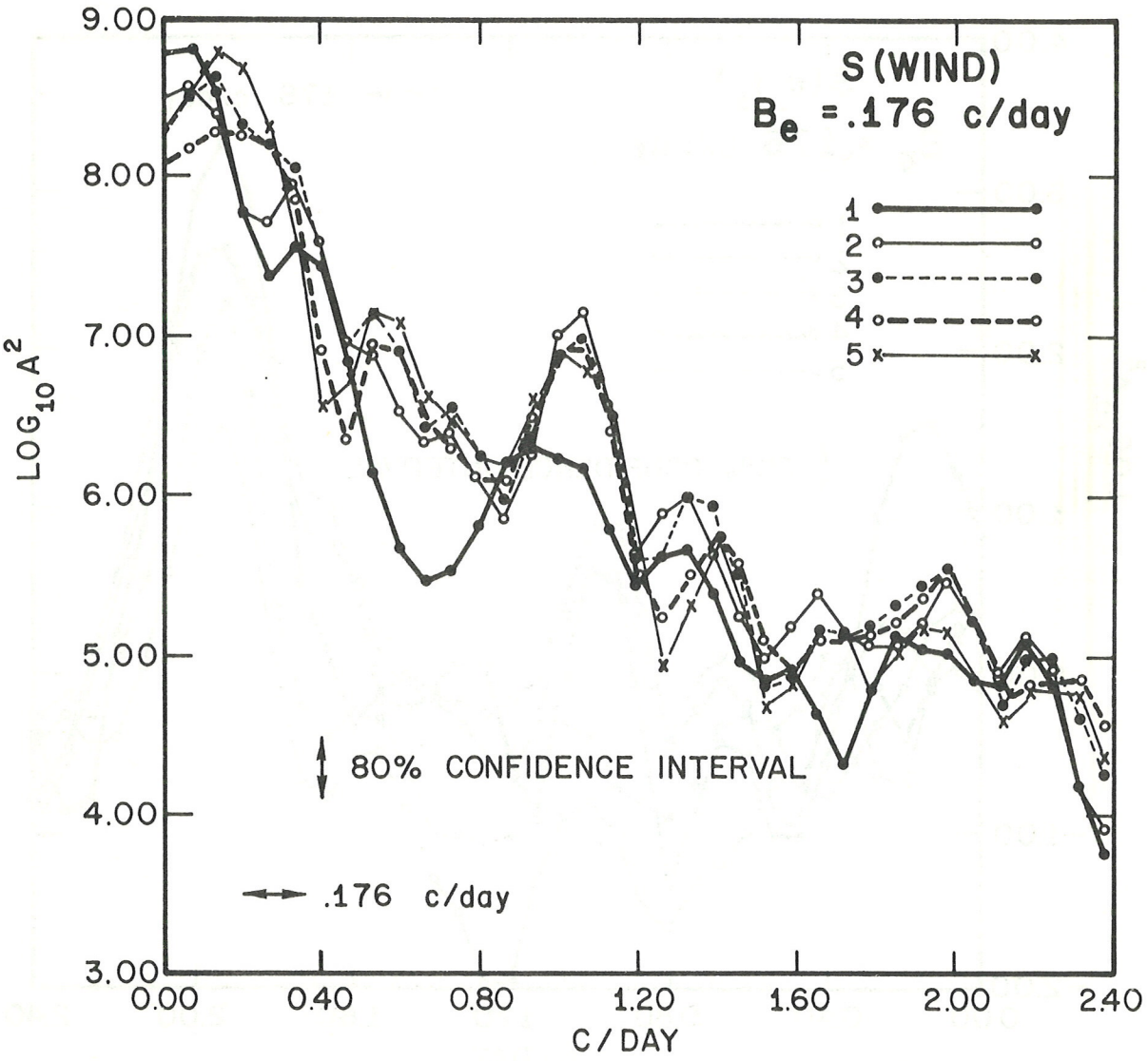

Figure 11c. Spectra of north component of wind for five record lengths of 1024 hours. Each record length overlaps its adjacent record length by 77%.

wind. The spectra computed in figures 8 and 10 represent a synthesis of the nonstationary features in figure 11.

The overall tendency of the spectra is for the energy to shift about in the low frequency part of the spectrum. This can be seen for all three parameters, the north component of current at V1, the east-west heat flux, and the wind. In some instances, the daily variations appear to be partially masked by the low frequency part of the spectrum except for the wind which has a fairly distinct and stationary diurnal peak.

6. CONCLUSIONS

The histograms of direction from all three stations show a clearly defined north-south fluctuation for the low frequency motions. The high frequency motions tend to flatten out the distribution of low frequency directions. This is caused by the east-west tidal current movements associated with the proximity of coastal inlets to these stations.

Shallow water motions (less than 20 m) tend to be driven largely by the wind for low frequency forcing (periods longer than several days) with negligible lag.

In shallow water the mean vertical velocity shear near mid-depth is on the order of 10^{-2} to 5 $(10)^{-2}$ sec^{-1}, and data suggest that single point measurements characterize water column motions since linear correlations between components of upper and lower sensors were very near 0.9.

Motions with periods of 10 days or less can be attributed to both the Florida Current and the wind forcing.

Temperature can be used as a tracer of coastal water during the winter and early spring where, on the average, the temperature gradient is positive to the east. This appears to be caused by frequently occurring cold fronts (every 1 to 2 weeks) that lower the temperature of the shallow shelf water. Occasionally, however, the temperature gradient will change sign (see fig. 7) when too few cold front events of sufficient intensity occur, allowing a rise in the temperature of the inshore waters even in winter.

Near the shelf break (station V3), there appears to be a temperature drop associated with southerly flow for the two southerly flow events recorded at station V3.

The dominant east-west divergences of heat flux are associated with the slowly varying processes, that is,

$$\frac{1}{h} \nabla_x \cdot (\langle \bar{u}\, \bar{t} \rangle h) \sim 0(3(10)^{-6}), {}^{o}C/sec;$$

with the tidal inlet effects removed, the divergence of the high frequency term

$$\frac{1}{h} \nabla_x \cdot (\langle u't' \rangle h) \sim 0(2(10)^{-7}), {}^{o}C/sec$$

is an order of magnitude smaller. This suggests that the scale length for spatial variation of east-west heat flux is larger than the distance between V1 and V2.

The dominant momentum flux divergence is at low frequency,

$$\frac{1}{h}\nabla_x . (\langle \bar{v}\ \bar{u} \rangle h) \sim 0(2(10)^{-4}) \text{ cm/sec}^2 .$$

The remaining divergences of $\langle \bar{u}\ \bar{u} \rangle$, $\langle v'u' \rangle$, and $\langle u'u' \rangle$ vary between $2(10)^{-5}$ and $5(10)^{-5}$, where $\langle v'u' \rangle$ and $\langle u'u' \rangle$ are the fluxes with the tidal effects removed; thus, it seems that the shallow water shelf dynamics are controlled mainly by the low frequency heat and momentum exchange.

The major problem in computing the statistics of South Florida coastal processes is one of adequate sampling or sufficient record length. It is estimated that at least 4 months of record are needed for stability of the computations.

Spectra of the data show basically nonstationary low frequency forcing of the shelf water by the wind and the Florida Current.

7. REFERENCES

Goodheart, A. J. (1966): ODESSA, presented at the World Meteorology Organization Technical Conference on Automatic Weather Systems, Sept. 1966, Geneva, Switzerland, TCAWS/Doc. 28 (8.VII.1966); also in (1968): ODESSA, small buoys with big voices, Special Report: Instrumentation, Ocean Industry 3(10):55-59.

Jenkins, G. M., and D. G. Watts (1969): Spectral Analysis and Its Application, San Francisco, Holden-Day, 525 pp.

Lee, T. N. (1973): "Florida Current Spin-Off Eddies," Ph.D Dissertation, Florida State University, Tallahassee, 92 pp.

☆U.S. GOVERNMENT PRINTING OFFICE: 1975 — 677-347 / 1225 REGION NO. 8

ENVIRONMENTAL RESEARCH LABORATORIES

The mission of the Environmental Reasearch Laboratories is to study the oceans, inland waters, the lower and upper atmosphere, the space environment, and the earth, in search of the understanding needed to provide more useful services in improving man's prospects for survival as influenced by the physical environment. Laboratories contributing to these studies are:

Atlantic Oceanographic and Meteorological Laboratories (AOML): Geology and geophysics of ocean basins and borders, oceanic processes, sea-air interactions and remote sensing of ocean processes and characteristics (Miami, Florida).

Pacific Marine Environmental Laboratory (PMEL): Environmental processes with emphasis on monitoring and predicting the effects of man's activities on estuarine, coastal, and near-shore marine processes (Seattle, Washington).

Great Lakes Environmental Research Laboratory (GLERL): Physical, chemical, and biological, limnology, lake-air interactions, lake hydrology, lake level forecasting, and lake ice studies (Ann Arbor, Michigan).

Atmospheric Physics and Chemistry Laboratory (APCL): Processes of cloud and preciptation physics; chemical composition and nucleating substances in the lower atmosphere; and laboratory and field experiments toward developing feasible methods of weather modification.

Air Resources Laboratories (ARL): Diffusion, transport, and dissipation of atmospheric contaminants; development of methods for prediction and control of atmospheric pollution; geophysical monitoring for climatic change (Silver Spring, Maryland).

Geophysical Fluid Dynamics Laboratory (GFDL): Dynamics and physics of geophysical fluid systems; development of a theoretical basis, through mathematical modeling and computer simulation, for the behavior and properties of the atmosphere and the oceans (Princeton, New Jersey).

National Severe Storms Laboratory (NSSL): Tornadoes, squall lines, thunderstorms, and other severe local convective phenomena directed toward improved methods of prediction and detection (Norman, Oklahoma).

Space Environment Laboratory (SEL): Solar-terrestrial physics, service and technique development in the areas of environmental monitoring and forecasting.

Aeronomy Laboratory (AL): Theoretical, laboratory, rocket, and satellite studies of the physical and chemical processes controlling the ionosphere and exosphere of the earth and other planets, and of the dynamics of their interactions with high-altitude meteorology.

Wave Propagation Laboratory (WPL): Development of new methods for remote sensing of the geophysical environment with special emphasis on optical, microwave and acoustic sensing systems.

Marine EcoSystem Analysis Program Office (MESA): Plans and directs interdisciplinary analyses of the physical, chemical, geological, and biological characteristics of selected coastal regions to assess the potential effects of ocean dumping, municipal and industrial waste discharges, oil pollution, or other activity which may have environmental impact.

Weather Modification Program Office (WMPO): Plans and directs ERL weather modification research activities in precipitation enhancement and severe storms mitigation and operates ERL's research aircraft.

NATIONAL OCEANIC AND ATMOSPHERIC ADMINISTRATION
BOULDER, COLORADO 80302